Extinction cross section of an arbitrary body in a viscous incompressible fluid

Scott A. Wymer, Akhlesh Lakhtakia, and Renata S. Engel
Department of Engineering Science and Mechanics, The Pennsylvania State University, University Park, Pennsylvania 16802-1401
(Received 12 December 1994)

When analyzing time-dependent Stokesian flow around an arbitrary body in terms of time-harmonic phasors, analytic techniques commonly used for frequency-domain scattering can be brought to bear. A common measure of the scattering response of a body is the extinction cross section. However, as the wave number for a Stokesian flow is necessarily complex, the usual interpretation of the extinction cross section is untenable for this problem. It is shown here that a detector-based interpretation of the extinction cross section is unambiguous and experimentally relevant. An almost exact formula is derived for the extinction cross section for flow around an arbitrary body. Computed values for the cross section are presented for a spherical body using two different boundary condition cases: pure stick (i.e., no slip) and pure slip.

PACS number(s): 47.50.+d

I. INTRODUCTION

Frequency-domain treatments of boundary-value problems are commonplace in electromagnetism and there is significant mathematical unity between electromagnetism and fluid mechanics [1,2]. Therefore, when the equations describing the flow of a slow viscous fluid are transformed to frequency space, a large number of techniques commonly employed for electromagnetic scattering become available. This was noticed by Felderhof about two decades ago [3,4] and he has since played a major role in the use of scattering techniques for solving boundary-value problems in fluid mechanics [5,6].

Typically, in fluid mechanics, when a body is imposed in a flow field, the flow is described using solutions for the total velocity and pressure fields that incorporate the consequence of the body's presence [7,8]. When examining the flow field using a scattering approach, the total velocity and pressure fields must be broken up into two parts: a specified incident field and a scattered field. The scattered field as well as the incident field are expanded as series of appropriate basis functions. The coefficients of expansion of the scattered field are related to those of the incident field via a matrix operator. This matrix operator is dependent on (i) the frequency; (ii) the shape, the size, and the constitutive relations of the scattering body; (iii) the constitutive relations of the fluid; and (iv) the boundary conditions prevailing at the bimaterial interface. Let us also note the use of this approach in fluid statics [9].

One measure used to describe the effects of a scattering body in an incident field is the extinction cross section C_{ext}. The extinction cross section has its basis in the principle of conservation of energy. In electromagnetism and acoustics, a common analytic method for calculating C_{ext} is to examine the energy flux change, due to the presence of a scattering body, on the surface of an arbitrary bounding region [10,11]. When the ambient medium is absorbing, the energy loss due to absorption becomes dependent upon the volume of the bounding region; therefore, no method can be used that requires the integration over some arbitrary bounding region. An alternative method is to consider the energy received upon the surface of a detector placed in the forward scattering direction [12]. The energy received by a detector is altered due to the presence of the body. The extinction cross section is equivalent to the area of the detector that would have to be covered up or removed to give an energy alteration equivalent to that due to the presence of the scattering body in the field. This alternative, detector-based, approach has been used in the electromagnetism literature [13,14]. Since the wave number in fluid mechanics is complex, the classical approach [10] will not work; but the detector-based method will, and it forms the basis for this paper.

The extinction cross section is quantitated in the alternative, detector-based, approach as

$$C_{\text{ext}}=(U-U_i)\frac{A_d}{U_i} \ . \tag{1}$$

Here U is the rate of change of the energy normally incident on a planar detector of area A_d when the scattering body is present and U_i is the rate of change of energy normally incident on the detector when the body is not present. The formulation for C_{ext} presented here is valid for any arbitrary body.

II. PRELIMINARY ANALYSIS

Time-dependent, incompressible, viscous flow is governed by the equation for the conservation of momentum and the continuity equation

$$\rho\frac{D\tilde{\mathbf{v}}(\mathbf{r},t)}{Dt}-\mu\nabla^2\tilde{\mathbf{v}}(\mathbf{r},t)+\nabla\tilde{p}(\mathbf{r},t)=0 \ , \tag{2a}$$

$$\nabla\cdot\tilde{\mathbf{v}}(\mathbf{r},t)=0 \ . \tag{2b}$$

Here ρ is the mass density and μ is the coefficient of viscosity; $\tilde{\mathbf{v}}(\mathbf{r},t)$ is the velocity vector and $\tilde{p}(\mathbf{r},t)$ is the pressure, both functions of the position $\mathbf{r}$ and time t; D/Dt is the *material* time derivative. In order for us to

apply scattering techniques, these equations must be linearized by setting the convective acceleration to zero. Then we obtain the two equations

$$\rho\frac{\partial\tilde{\mathbf{v}}(\mathbf{r},t)}{\partial t}-\mu\nabla^2\tilde{\mathbf{v}}(\mathbf{r},t)+\nabla\tilde{p}(\mathbf{r},t)=0\ , \tag{3a}$$

$$\nabla\cdot\tilde{\mathbf{v}}(\mathbf{r},t)=0\ , \tag{3b}$$

of which the first one describes Stokesian flow. When harmonic time dependence is assumed, i.e.,

$$\begin{aligned}\tilde{\mathbf{v}}(\mathbf{r},t)&=\mathrm{Re}[\mathbf{v}(\mathbf{r})e^{-i\omega t}]\ ,\\ \tilde{p}(\mathbf{r},t)&=\mathrm{Re}[p(\mathbf{r})e^{-i\omega t}]\ ,\end{aligned} \tag{4}$$

with $i\equiv\sqrt{(-1)}$ while $\mathbf{v}(\mathbf{r})$ and $p(\mathbf{r})$ are phasors, (3a) becomes

$$k^2\mathbf{v}(\mathbf{r})+\nabla^2(\mathbf{r})-\frac{1}{\mu}\nabla p(\mathbf{r})=0\ , \tag{5}$$

where

$$k=\frac{(i+1)}{\sqrt{2}}\left[\frac{\omega\rho}{\mu}\right]^{1/2} \tag{6}$$

is the complex wave number. Equation (3b) transforms likewise to

$$\nabla\cdot\mathbf{v}(\mathbf{r})=0\ . \tag{7}$$

Thus time-dependent flow has been formulated in the frequency (ω) domain; see also a review paper by Criminale and Smith [15]. Equations (5) and (7) can be solved using spherical harmonic expansions of $\mathbf{v}(\mathbf{r})$ and $p(\mathbf{r})$ [3–8]. Very importantly, since the wave number k is complex, the fluid has to be treated as an absorbing medium in the context of scattering theory.

It is convenient in solving (5) and (7) to decompose the velocity phasor into a longitudinal component $\mathbf{v}_l$ and a solenoidal component $\mathbf{v}_t$:

$$\mathbf{v}=\mathbf{v}_l+\mathbf{v}_t,\quad \nabla\times\mathbf{v}_l=\mathbf{0},\quad \nabla\cdot\mathbf{v}_t=0\ . \tag{8}$$

Substituting these definitions into (5) and (7) leads to an equation for $\mathbf{v}_l$ and $\mathbf{v}_t$. After assuming

$$\mathbf{v}_l=\frac{1}{\mu k^2}\nabla p\ , \tag{9}$$

we obtain

$$\nabla^2\mathbf{v}_t+k^2\mathbf{v}_t=\mathbf{0}\ . \tag{10}$$

But $\nabla\cdot\mathbf{v}=0$ because of incompressibility, giving

$$\nabla^2 p=0\ . \tag{11}$$

Each of the three fields $\mathbf{v}_l(\mathbf{r})$, $\mathbf{v}_l(\mathbf{r})$, and $p(\mathbf{r})$ is expressed as the sum of scattered components ($\mathbf{v}_{l_{sc}}$, $\mathbf{v}_{t_{sc}}$, and p_{sc}) and incident components ($\mathbf{v}_{l_i}$, $\mathbf{v}_{t_i}$, and p_i). The incident fields exist when the scattering body is not present. For this work the incident field is chosen to be a plane, transverse velocity wave propagating along the z axis. In choosing a purely transverse incident wave we eliminate the consideration of any incident pressure; thus

$$\mathbf{v}_i(\mathbf{r})=\mathbf{V}e^{ikz},\quad p_i=0 \tag{12}$$

with $\mathbf{V}\cdot\hat{\mathbf{z}}=0$. Here and hereafter every unit vector is decorated with a caret and the Cartesian as well as the spherical coordinate systems have been used.

Parenthetically, we observe that (10), a Helmholtz equation, bears comparison with the differential equation governing the electric field phasor in an isotropic dielectric medium. But (9) does not correspond to the equation satisfied by the velocity phasor of an acoustic wave propagating in an inviscid fluid. The reason is that the velocity phasor of the acoustic wave, although purely longitudinal, is not constrained by (7). As is clear from (11), the longitudinal velocity phasor in our work does not propagate.

III. POWER DENSITY CALCULATIONS

Since the wave number k for a Stokesian flow is complex, C_{ext} must be calculated using the detector-based approach mentioned in Sec. I. The detector is placed on the positive z axis, in the forward scattering direction (i.e., $\theta=0$) with its face perpendicular to the z axis, as shown in Fig. 1. We assume that the detector is planar and that it is placed far enough away from the body to allow far-zone approximations of the forward scattered field to be valid. In the far zone, the distance z_d to the detector is so large that the solid angle $\Omega_d=A_d/z_d^2$ subtended by the detector at the origin is small and thus only the forward scattered field is gathered by the detector. The maximum radius of the detector R_d is assumed large enough such that the detector can gather all of the forward scattered field to calculate the extinction cross section: $R_d\gg\sqrt{\pi z_d/2|k|}$.

For a viscous, incompressible fluid the rate of change

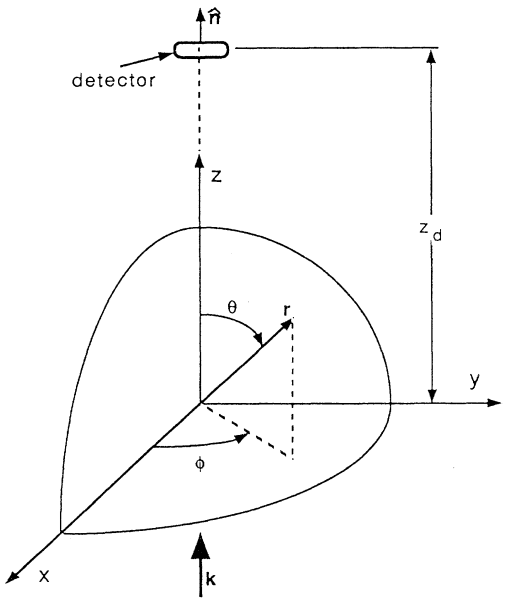

FIG. 1. Coordinate system used, showing the incident plane-wave direction.

of the energy per unit volume $E(\mathbf{r},t)$ can be expressed as

$$E(\mathbf{r},t)=\nabla\cdot[\tilde{\underline{\tau}}(\mathbf{r},t)\cdot\tilde{\mathbf{v}}(\mathbf{r},t)-\tilde{p}(\mathbf{r},t)\tilde{\mathbf{v}}(\mathbf{r},t)] , \tag{13}$$

where the shear stress tensor $\tilde{\underline{\tau}}(\mathbf{r},t)$ is defined by

$$\tilde{\underline{\tau}}(\mathbf{r},t)=\mu[\nabla\tilde{\mathbf{v}}(\mathbf{r},t)+\tilde{\mathbf{v}}(\mathbf{r},t)\nabla] . \tag{14}$$

Let

$$\begin{aligned}\mathbf{S}(\mathbf{r})&\equiv\langle\tilde{\underline{\tau}}(\mathbf{r},t)\cdot\tilde{\mathbf{v}}(\mathbf{r},t)-\tilde{p}(\mathbf{r},t)\tilde{\mathbf{v}}(\mathbf{r},t)\rangle_t\\&=\tfrac{1}{2}\mathrm{Re}[\underline{\tau}(\mathbf{r})\cdot\mathbf{v}^*(\mathbf{r})-p(\mathbf{r})\mathbf{v}^*(\mathbf{r})]\end{aligned} \tag{15}$$

be the total time-averaged power flux density, $\underline{\tau}$ being the phasor analog of $\tilde{\underline{\tau}}$ while the asterisk denotes the complex conjugate. Now we can define the rate of change of energy U on the detector's surface in terms of $\mathbf{S}(\mathbf{r})$ as

$$U=\int_{A_d}\mathbf{S}(\mathbf{r})\cdot\hat{\mathbf{n}}\,dA , \tag{16}$$

where $\hat{\mathbf{n}}$ is the unit normal to the detector's surface. For a planar detector located in the forward direction, $\hat{\mathbf{n}}=\hat{\mathbf{z}}\approx\hat{\mathbf{r}}$ over the detector surface because $\Omega_d\ll 1$; thus (16) may be approximated to

$$U=\int_{A_d}\hat{\mathbf{r}}\cdot\mathbf{S}(z_d\hat{\mathbf{z}})dA . \tag{17}$$

The field quantities $\underline{\tau}$, $\mathbf{v}$, and p are all written as the sum of incident and scattered contributions: $\mathbf{v}=\mathbf{v}_i+\mathbf{v}_{sc}$, $p=p_i+p_{sc}$, and $\underline{\tau}=\underline{\tau}_i+\underline{\tau}_{sc}$. Then,

$$\mathbf{S}=\tfrac{1}{2}\mathrm{Re}[(\underline{\tau}_i\mathbf{v}_i^*-p_i\mathbf{v}_i^*)+(\underline{\tau}_{sc}\cdot\mathbf{v}_{sc}^*-p_{sc}\mathbf{v}_{sc}^*) \tag{18}$$

$$+(\underline{\tau}_{sc}\cdot\mathbf{v}_i^*+\underline{\tau}_i^*\cdot\mathbf{v}_{sc}-p_{sc}\mathbf{v}_i^*-p_i^*\mathbf{v}_{sc})] . \tag{19}$$

For convenience let us break $\mathbf{S}$ up into three components

$$\mathbf{S}_i=\tfrac{1}{2}\mathrm{Re}[\underline{\tau}_i\mathbf{v}_i^*-p_i\mathbf{v}_i^*] , \tag{20}$$

$$\mathbf{S}_{\mathrm{I}}=\tfrac{1}{2}\mathrm{Re}[\underline{\tau}_{sc}\cdot\mathbf{v}_{sc}^*-p_{sc}\mathbf{v}_{sc}^*] , \tag{21}$$

$$\mathbf{S}_{\mathrm{II}}=\tfrac{1}{2}\mathrm{Re}[\underline{\tau}_{sc}\cdot\mathbf{v}_i^*+\underline{\tau}_i^*\cdot\mathbf{v}_{sc}-p_{sc}\mathbf{v}_i^*-p_i^*\mathbf{v}_{sc}] . \tag{22}$$

Here $\mathbf{S}_i$ is the power flux density due only to the incident field and $\mathbf{S}_{\mathrm{I}}$ is the power flux density solely due to the scattered field.

With the incident wave defined in (12), the shear stress $\underline{\tau}_i$ due to the incident field becomes

$$\underline{\tau}_i=ik\mu(\mathbf{V}\hat{\mathbf{z}}+\hat{\mathbf{z}}\mathbf{V})e^{ikz} . \tag{23}$$

We can orient our coordinate axes such that $\mathbf{V}=V\hat{\mathbf{x}}$ without loss of generality; hence

$$\underline{\tau}_i=ik\mu V(\hat{\mathbf{x}}\hat{\mathbf{r}}+\hat{\mathbf{r}}\hat{\mathbf{x}})e^{ikz} . \tag{24}$$

Only the radial component of $\mathbf{S}$ appears in (17); therefore, using the definitions for shear stress, (14) and (23), we obtain

$$\begin{aligned}\hat{\mathbf{r}}\cdot\mathbf{S}_i&=\frac{\mu}{2}\mathrm{Re}[(ik)e^{i(k-k^*)z}]|V|^2\\&=-\frac{\mu}{2}e^{-2\,\mathrm{Im}[k]z}|V|^2\mathrm{Im}[k] ,\end{aligned} \tag{25}$$

$$\hat{\mathbf{r}}\cdot\mathbf{S}_{\mathrm{I}}=\tfrac{1}{2}\mathrm{Re}\left\{\mu\left[(\mathbf{v}_{sc}^*\cdot\nabla)(\hat{\mathbf{r}}\cdot\mathbf{v}_{sc})+\mathbf{v}_{sc}^*\cdot\left[\frac{\partial\mathbf{v}_{sc}}{\partial r}\right]\right]-\hat{\mathbf{r}}\cdot\mathbf{v}_{sc}^*p_{sc}\right\} , \tag{26}$$

$$\hat{\mathbf{r}}\cdot\mathbf{S}_{\mathrm{II}}=\tfrac{1}{2}\mathrm{Re}\left\{e^{-ik^*z}V^*\left[\mu\left[(\hat{\mathbf{x}}\cdot\nabla)(\hat{\mathbf{r}}\cdot\mathbf{v}_{sc})+\hat{\mathbf{x}}\cdot\frac{\partial\mathbf{v}_{sc}}{\partial r}-\hat{\mathbf{x}}\cdot(ik^*\mathbf{v}_{sc}+\hat{\mathbf{r}}\hat{\mathbf{r}}\cdot\mathbf{v}_{sc})\right]-(\hat{\mathbf{x}}\cdot\hat{\mathbf{r}})p_{sc}\right]\right\} \tag{27}$$

in the forward direction.

IV. FAR-ZONE APPROXIMATION

As our detector lies far from the scattering body, the far-zone approximation (i.e., $|k|r\to\infty$) of the scattered field quantities may be used. We need to examine the asymptotic behavior in $|k|r$ of three quantities (i.e., $\mathbf{v}_{sc}$, $\partial\mathbf{v}_{sc}/\partial r$ and p_{sc}) keeping in mind that the behavior with respect to kr of $\mathbf{v}_{sc}$ is different for its longitudinal and solenoidal components (see the Appendix). In making the far-zone approximation, we discard all those terms of order $(kr)^{-2}$ and smaller. From the scattered field expansions given in the Appendix, we see that

$$\mathbf{v}_{sc_l}(\mathbf{r})\underset{|k|r\gg1}{\sim}\mathbf{0} , \tag{28}$$

$$\mathbf{v}_{sc}(\mathbf{r})\underset{|k|r\gg1}{\sim}\frac{e^{ikr}}{kr}\mathbf{g}_1(\hat{\mathbf{r}}) , \tag{29}$$

$$\frac{\partial\mathbf{v}_{sc}(\mathbf{r})}{\partial r}\underset{|k|r\gg1}{\sim}\frac{e^{ikr}}{kr}\mathbf{g}_2(\hat{\mathbf{r}}) , \tag{30}$$

$$p_{sc}(\mathbf{r})\underset{|k|r\gg1}{\sim}\frac{1}{kr}(\mu D') , \tag{31}$$

where D' is a constant and is defined along with the vector functions $\mathbf{g}_1(\hat{\mathbf{r}})$ and $\mathbf{g}_2(\hat{\mathbf{r}})$ in the Appendix [Eqs. (A4) and (A5)].

These limiting expressions allow us to simplify (26) and (27) to

$$\hat{\mathbf{r}}\cdot\mathbf{S}_{\mathrm{I}}\approx\frac{\mu}{2}\mathrm{Re}\left[\frac{\exp(-2\,\mathrm{Im}[k]r)}{|k|^2r^2}\mathbf{g}_1^*(\hat{\mathbf{r}})\cdot\mathbf{g}_2(\hat{\mathbf{r}})\right] , \tag{32}$$

$$\hat{\mathbf{r}}\cdot\mathbf{S}_{\mathrm{II}}\approx\frac{\mu}{2}\mathrm{Re}\left[\exp\left[-2\,\mathrm{Im}[k]z\right]\frac{e^{ik(r-z)}}{kr}\times V^*\hat{\mathbf{x}}\cdot[\mathbf{g}_2(\hat{\mathbf{r}})-ik^*\mathbf{g}_1(\hat{\mathbf{r}})]-\frac{e^{-ik^*z}}{kr}V^*(\hat{\mathbf{r}}\cdot\hat{\mathbf{x}})D'\right] \tag{33}$$

for locations on the detector. But $\hat{\mathbf{r}}\approx\hat{\mathbf{z}}$ on the detector and $\mathbf{g}_2(\hat{\mathbf{z}})=ik\mathbf{g}_1(\hat{\mathbf{z}})$; hence

$$\hat{\mathbf{r}}\cdot\mathbf{S}_{\mathrm{I}}=\frac{\mu}{2}\mathrm{Re}\left[ik|\mathbf{g}_1(\hat{\mathbf{z}})|^2\frac{\exp(-2\,\mathrm{Im}[k]r)}{|k|^2r^2}\right] \tag{34}$$

$$\hat{\mathbf{r}}\cdot\mathbf{S}_{\mathrm{II}} = -\mathrm{Im}[k]\mu \exp(-2\,\mathrm{Im}[k]z_d) \times \mathrm{Re}\left[V^*(\hat{\mathbf{x}}\cdot\mathbf{g}_1(\hat{\mathbf{z}})) \frac{e^{ik(r-z_d)}}{kr} \right] \tag{35}$$

on the detector.

V. EXTINCTION CROSS SECTION

Using (34) and (35) in (16) for U gives

$$U_{\mathrm{I}} = \frac{\mu}{2}\mathrm{Re}\left[ik|\mathbf{g}_1(\hat{\mathbf{z}})|^2 \int_{A_d} \frac{e^{-2\,\mathrm{Im}[k]r}}{|k|^2 r^2} dA \right] \tag{36}$$

$$\cong -\frac{\mu}{2}\left[\frac{e^{-2\,\mathrm{Im}[k]z_d}}{|k|^2 z_d^2} \right] A_d |\mathbf{g}_1(\hat{\mathbf{z}})|^2 \mathrm{Im}[k] , \tag{37}$$

$$U_{\mathrm{II}} = -\mathrm{Im}[k]\mu e^{-2\,\mathrm{Im}[k]z_d} \times \mathrm{Re}\left[V^*(\hat{\mathbf{x}}\cdot\mathbf{g}_1(\hat{\mathbf{z}})) \int_{A_d} \frac{e^{ik(r-z_d)}}{kr} dA \right] , \tag{38}$$

and

$$U_i = -\mu e^{-2\,\mathrm{Im}[k]z_d} \frac{A_d}{2} |V|^2 \mathrm{Im}[k] , \tag{39}$$

where U_i, U_{I}, and U_{II} correspond to $\mathbf{S}_i$, $\mathbf{S}_{\mathrm{I}}$, and $\mathbf{S}_{\mathrm{II}}$, respectively.

The remaining integral in U_{II} can be cast in the form

$$\int_{A_d} \exp\left[ikr\left[1 - \frac{z_d}{r} \right] \right] \left[\frac{1}{kr} \right] dx\, dy . \tag{40}$$

In the asymptotic limit $|k|r \to \infty$, this integral can be evaluated using the method of stationary phase [16]; thus

$$\int_{A_d} \frac{e^{ik(r-z_d)}}{kr} dx\, dy \cong \frac{2\pi i}{k^2} \tag{41}$$

and

$$U_{\mathrm{II}} = \mathrm{Im}[k]\mu e^{-2\,\mathrm{Im}[k]z_d} \mathrm{Im}\left[V^*(\hat{\mathbf{x}}\cdot\mathbf{g}_1(\hat{\mathbf{z}})) \left[\frac{2\pi}{k^2} \right] \right] . \tag{42}$$

In (1), we need $U - U_i = U_{\mathrm{I}} + U_{\mathrm{II}}$. But U_{I} is of the order $(|k|z_d)^{-2}$ and quantities of this order may be neglected in the far zone. Therefore, from (1) we get

$$C_{\mathrm{ext}} \cong \frac{U_{\mathrm{II}} A_d}{U_i} . \tag{43}$$

Using (39) and (42), we now get a very simple expression for the extinction cross section as

$$C_{\mathrm{ext}} \cong -\left[\frac{4\pi}{|V|^2} \right] \mathrm{Im}\left[\frac{V^*}{k^2} (\hat{\mathbf{x}}\cdot\mathbf{g}_1(\hat{\mathbf{z}})) \right] \tag{44}$$

$$\cong -4\pi\,\mathrm{Im}\left[\frac{\hat{\mathbf{x}}\cdot\mathbf{g}_1(\hat{\mathbf{z}})}{k^2 V} \right] . \tag{45}$$

It is usual in the electromagnetism literature to define a nondimensional quantity called the extinction efficiency Q_{ext}. This quantity is the ratio of the extinction cross section to the cross-sectional area of the scatterer projected on the plane to which the incident wave vector is perpendicular. Let this cross section area be equal to the area of a circle of radius a; then

$$Q_{\mathrm{ext}} \equiv \frac{C_{\mathrm{ext}}}{\pi a^2} \cong -4\,\mathrm{Im}\left[\frac{\hat{\mathbf{x}}\cdot\mathbf{g}_1(\hat{\mathbf{z}})}{(ka)^2 V} \right] \tag{46}$$

is the extinction efficiency.

VI. RESULTS FOR A SPHERICAL BODY

The spherical harmonic expansion of the incident wave (12) is shown in the Appendix as Eq. (A8). The scattered pressure and velocity fields are also written as expansions in terms of spherical harmonic functions; see Eqs. (A1)–(A3) in the Appendix.

The incident and the scattered expansion coefficients have to be related through the boundary conditions. In order to illustrate the developments of the previous sections, we considered two distinct sets of boundary conditions. For either set, the body was considered impermeable so that

$$\hat{\mathbf{n}}_b \cdot \mathbf{v} = \mathbf{0} \tag{47}$$

on the surface of the body, where $\hat{\mathbf{n}}_b$ is the unit vector normal to the surface of the scattering body. Next, as the flow tangential to the body must be described at the surface, we considered two separate cases: pure stick (i.e., no slip) and pure slip. For the pure stick case the tangential velocity is specified through

$$\hat{\mathbf{n}}_b \times \mathbf{v} = \mathbf{0} \tag{48}$$

and for the pure slip case we use

$$\hat{\mathbf{n}}_b \times [\tau\cdot\hat{\mathbf{n}}_b - p\hat{\mathbf{n}}_b] = \mathbf{0} . \tag{49}$$

Incidentally, although pure slip is only possible with an inviscid fluid and can be thus thought of as a mathematical artifact, it has physical meaning as a limiting case of mixed slip-stick boundary conditions; see, e.g., [9].

Upon application of the boundary condition sets to a spherical scatterer of radius a and subsequent use of the orthogonality properties of the angular functions in Eqs. (A1)–(A3) and (A8), the scattered field coefficients may be determined as

$$A^3_{mn\sigma} = \frac{-n(ka)^{n-1}}{h_{n-1}(ka)} \left[A^1_{mn\sigma} \left[\frac{(ka)^n + 1}{n+2} h_{n+1}(ka) \right] - iC^1_{mn\sigma} \right] , \tag{50}$$

$$B^3_{mn\sigma} = -B^1_{mn\sigma} \left[\frac{j_n(ka)}{h_n(ka)} \right] , \tag{51}$$

$$C^3_{mn\sigma} = -A^1_{mn\sigma} \left[\frac{2n+1}{n+1} \right] \left[\frac{(ka)^{n-1}}{h_{n-1}(ka)} \right] - C^1_{mn\sigma} \left[\frac{j_{n-1}(ka)}{h_{n-1}(ka)} \right] \tag{52}$$

for the pure stick case and

$$A^3_{mn\sigma}=\frac{n(ka)^n}{kah_n(ka)+h_{n-1}(ka)} \times\left[A^1_{mn\sigma}[kah_n(ka)-h_{n+1}(ka)]+C^1_{mn\sigma}\frac{1}{ka}\right], \tag{53}$$

$$B^3_{mn\sigma}=-B^1_{mn\sigma}\left[\frac{\frac{n+1}{ka}j_n(ka)-j_{n-1}(ka)}{\frac{n+1}{ka}h_n(ka)-h_{n-1}(ka)}\right], \tag{54}$$

$$C^3_{mn\sigma}=-A^1_{mn\sigma}\left[\frac{2n+1}{n+1}\right]\left[\frac{(ka)^{n-1}}{kah_n(ka)-h_{n-1}(ka)}\right] -C^1_{mn\sigma}\left[\frac{kaj_n(ka)+j_{n-1}(ka)}{kah_n(ka)+h_{n-1}(ka)}\right], \tag{55}$$

when the pure slip boundary condition prevails. In these expressions, $h_n(\ )$ is the spherical Hankel function of the first kind and of order n, while $j_n(\ )$ is the spherical Bessel function of order n. With these scattered coefficients we calculated $\mathbf{g}_1(\hat{\mathbf{z}})$ and subsequently Q_{ext}. Values of the scattering efficiency were calculated for both the pure slip and pure stick boundary conditions using values for the normalized radius $|k|a$ of the sphere in the range $(0.5\le|k|a\le 50)$.

Before generating meaningful values for Q_{ext}, we first had to confirm that the series in Eq. (A6) converges within a preset tolerance limit in a finite number of terms. Figure 2 depicts convergence studies for three different values of $|k|a$. The percent error shown in Figs. 2 and 3 was calculated as

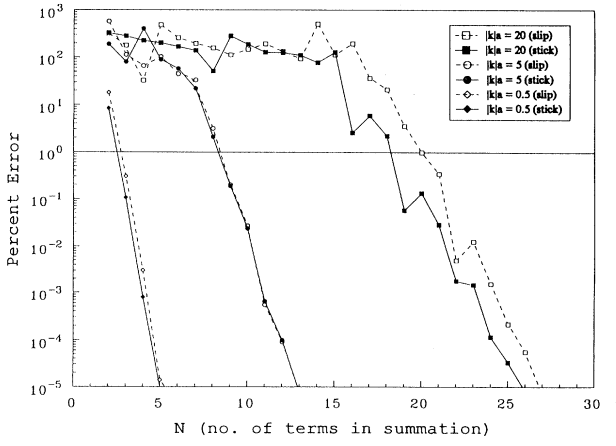

FIG. 2. Illustration of the convergence of (46) for three different values of $|k|a$ for pure slip and pure stick boundary condition sets, the scatterer being a sphere of radius a. The horizontal reference line represents $\pm 1\%$ error. Percent error shown is calculated using (56).

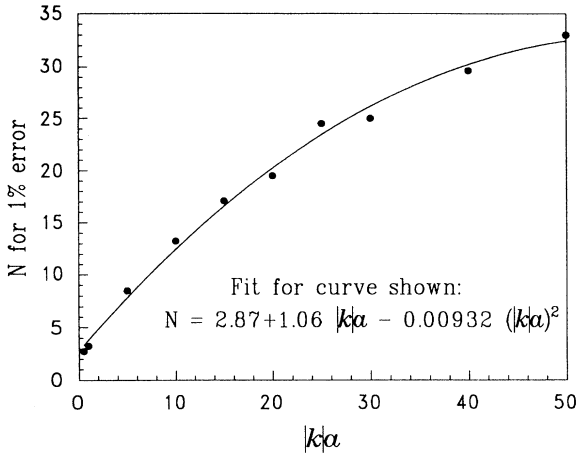

FIG. 3. Number of terms N required to compute Q_{ext} to within $\pm 1\%$ error. The slip boundary condition set was used for these calculations. The fitted quadratic curve gives estimates for adequate values of N as a function of $|k|a$ for a sphere of radius a.

$$100\times\frac{\text{Im}\left[\sum_{n=1}^{N}\hat{\mathbf{x}}\cdot\mathbf{g}_{1_n}\right]-\text{Im}\left[\sum_{n=1}^{N-1}\hat{\mathbf{x}}\cdot\mathbf{g}_{1_n}\right]}{\text{Im}\left[\sum_{n=1}^{N-1}\hat{\mathbf{x}}\cdot\mathbf{g}_{1_n}\right]}, \tag{56}$$

with $\mathbf{g}_{1_n}$ defined in Eq. (A6). As $|k|a$ increases, the number of terms N required for convergent values of Q_{ext} increases also. Since, as seen in Fig. 2, the pure slip case is the slower one of the two sets of boundary conditions to converge, we obtained an estimate for a minimum number of terms required for convergence for either case from examination of the slip case alone. The number of terms N required for $\pm 1\%$ error in convergence is shown in Fig. 3, for the pure slip case, when $|k|a\le 50$. A polynomial fit to the curve in Fig. 3 shows that $N=2.87+1.06|k|a-0.009\,32(|k|a)^2$ is adequate to achieve convergence to within $\pm 1\%$ error for $0.5\le|k|a\le 50$.

With knowledge of the series convergence established, Q_{ext} was computed with confidence. The behavior of Q_{ext} varies considerably for large $|k|a$ and for $|k|a\to 0$, the specific choices of the set of boundary conditions notwithstanding.

For large values of $|k|a$, Q_{ext} is a rapidly increasing, oscillatory function. This behavior is shown in Figs. 4 and 5 for the stick and slip cases, respectively. The sequence of plots in both of these figures shows the same data for Q_{ext} plotted on successively smaller scales in order to show the details of the oscillations. These sequences of plots demonstrate the oscillatory nature of Q_{ext} over a range $0\le|k|a\le 20$ and similar plots were obtained for higher values of $|k|a$.

The data points in Fig. 6 represent the positive and negative extrema of Q_{ext} with respect to $|k|a$ for both

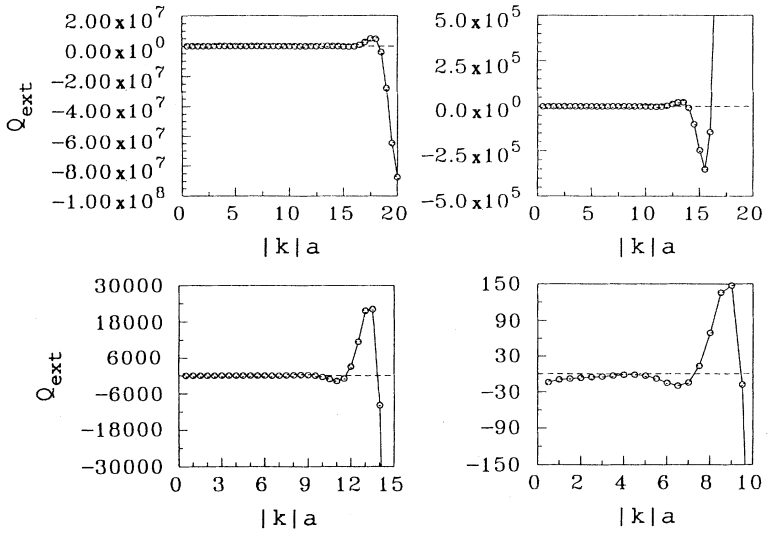

FIG. 4. Q_{ext} for the pure stick case as a function of $|k|a$; the multiple plots show the same data plotted on axes scaled successively smaller.

boundary condition sets (see also Table I). When these extrema are plotted together on a semilogarithmic graph, as shown in Fig. 6, the envelopes of the oscillations of Q_{ext} turn out to be exponential functions of the form $Ae^{B|k|a}$. For large values of $|k|a$, $|Q_{\text{ext}}|$ for the stick case shows positive and negative peak values over two orders of magnitude larger than $|Q_{\text{ext}}|$ for the slip case.

In order to examine the limiting case $|k|a \to 0$, we can substitute the low-argument approximations for the spherical Bessel and Hankel functions [17] in (50) and (53). When these coefficients are then substituted into Eq. (A4), we get

$$\mathbf{g}_1(\hat{\mathbf{r}}) \underset{|k|a\to 0}{\sim} -\frac{3V}{2}(ka)[\cos\theta\cos\phi\hat{\theta}-\sin\phi\hat{\phi}]+O((ka)^3) \tag{57}$$

for the pure stick case and

$$\mathbf{g}_1(\hat{\mathbf{r}}) \underset{|k|a\to 0}{\sim} -\frac{3V}{4}(ka)[\cos\theta\cos\phi\hat{\theta}-\sin\phi\hat{\phi}]+O((ka)^3) \tag{58}$$

for the pure slip case. On using these limiting expressions in (46), we obtain

$$Q_{\text{ext}} \underset{|k|a\to 0}{\sim} -3\sqrt{2}\frac{1}{|k|a} \tag{59}$$

for the pure stick case and

$$Q_{\text{ext}} \underset{|k|a\to 0}{\sim} -\frac{3\sqrt{2}}{2}\frac{1}{|k|a} \tag{60}$$

for the pure slip case. Calculated values for Q_{ext} are potted in Fig. 7 for values of $|k|a < 1$. Throughout this region of low $|k|a$ values, $Q_{\text{ext}} < 0$ for both sets of boundary conditions.

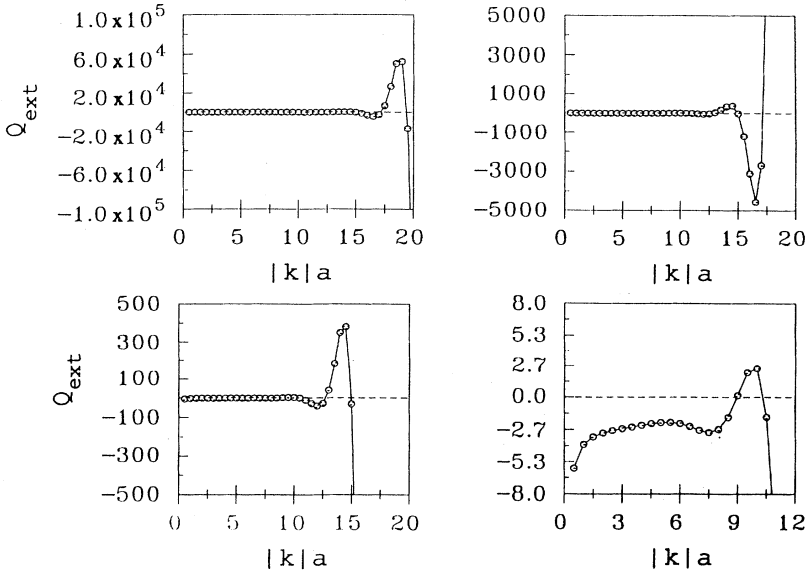

FIG. 5. Q_{ext} for the pure slip case as a function of $|k|a$; the multiple plots show the same data plotted on axes scaled successively smaller.

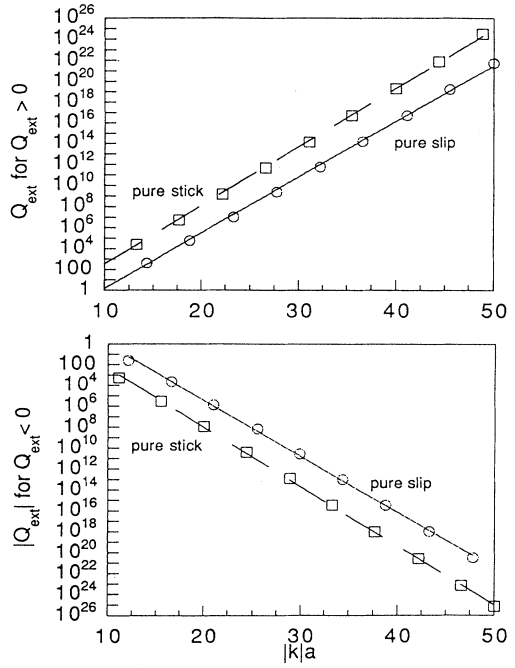

FIG. 6. Positive extrema of Q_{ext} are shown in the top graph, the negative on the bottom. Data from the calculations shown in Figs. 4 and 5 were used to generate these graphs.

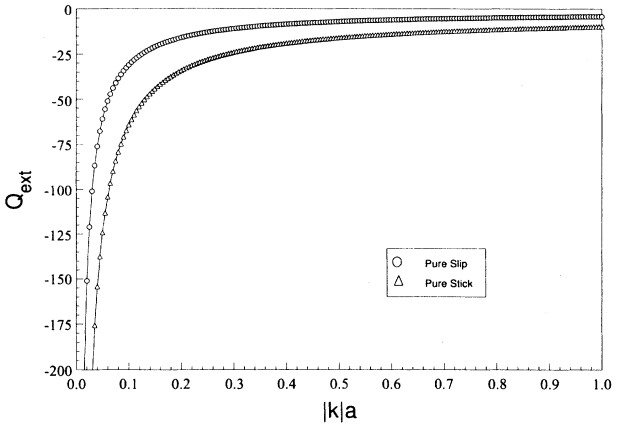

FIG. 7. Q_{ext} for small spherical scatterers. Note that $Q_{ext} \propto (|k|a)^{-1}$ when $|k|a \ll 1$.

An interesting difference between electromagnetism and fluid mechanics is afforded by the small $|k|a$ expressions. In electromagnetic parlance, $\mathbf{g}_1(\hat{\mathbf{r}})$ is called the far-zone scattering amplitude and it is proportional to $(ka)^3$ for the so-called electrically small scatterers (i.e., $|k|a \ll 1$). Hence Q_{ext} is proportional to $|k|a$ when $|k|a \ll 1$; see [12]. What we observed from (57) and (58) is that $\mathbf{g}_1(\hat{\mathbf{r}})$ is proportional to ka, and Q_{ext} therefore to $1/|k|a$, for small scatterers in a Stokesian flow. The scattering amplitude of a small scatterer is proportional to its volume for electromagnetic scattering, but turns out to be proportional to the cube root of its volume for the scattering of Stokesian flow. This observation needs further verification for nonspherical scatterers immersed in a Stokesian flow.

VII. DISCUSSION AND CONCLUSIONS

Because of the similarities in the formulation of electromagnetics and Stokesian flow, we applied analytic methods commonly reserved for electromagnetics to fluid flow problems. Using frequency-domain scattering methods to analyze the effect an arbitrary body will have when placed in a Stokesian flow, we derived a simple formula for the extinction cross section of the body. A transverse incident plane wave flow was assumed and all fields were expanded in spherical harmonics and simplified using the far-zone approximation. The special case of a spherical scatterer was investigated.

Both negative and positive values of Q_{ext} are found in Figs. 4, 5, and 7. The Stokesian flow is inherently absorbing or lossy due to viscous friction. This absorption is responsible for the wave number k being complex valued. The presence of absorption tells us that attenuation takes place in the fluid even without the presence of a scattering body.

When a body is placed in such an absorbing medium, negative values of Q_{ext} are possible and can be explained satisfactorily as follows. If the scattering body is less absorbing than the surrounding medium, more energy may be intercepted by the detector when the scattering body is present than when it is absent [13]. The presence of a body having less absorption than the surrounding medium may reduce the overall attenuation of a plane wave propagating in the medium, thus allowing higher fields at the detector.

We also considered two different sets of boundary conditions: pure slip and pure stick. The extinction efficiency behaves similarly as a function of $|k|a$ for either

TABLE I. Exponential fit parameters for the envelope of the local maxima of Q_{ext} as shown in Fig. 6 (the equation being fitted is $|Q_{ext}| = Ae^{B|k|a}$).

Fit parameter	Stick case		Slip case	
	$Q_{ext} > 0$	$Q_{ext} < 0$	$Q_{ext} > 0$	$Q_{ext} < 0$
A	8.177×10^{-4}	1.126×10^{-3}	6.917×10^{-6}	6.580×10^{-6}
B	1.290	1.283	1.227	1.227

set. The major difference is that the pure stick case shows consistently higher values of $|Q_{\text{ext}}|$ than the pure slip case for the same $|k|a$. The slip boundary conditions are defined, in part, by setting the friction on the surface of the scatterer to zero. Therefore, the difference in extinction between the two sets of boundary conditions is caused by the presence of viscous friction on the surface of the scattering body when the pure stick boundary conditions prevail.

The concept of the extinction cross section is valid for any body immersed in a Stokesian flow into which a transverse incident velocity wave is launched. The extinction cross section is a direct measure of the influence a body has on the launched flow and as such can be used to predict the effect of imposing a body in a flow. Our detector-based approach for extinction cross section is similar to insertion-loss measurements common-place in the areas of microwave and acoustic circuitry. Similar measurements may be possible in fluid mechanics if the spectral contents of the source and the detected signals are analyzed. As extinction cross section has found wide use in electromagnetism, we hope that it will find many applications in fluid dynamics also.

APPENDIX

Outside the minimum sphere circumscribing the body, the scattered fields due to an arbitrary body can be expanded in terms of spherical harmonic functions [2,16] that are regular at infinity as

$$p_{\text{sc}}(\mathbf{r})=\mu k \sum_{n=0}^{\infty}\sum_{m=0}^{n}\sum_{\sigma=e,o} A^3_{mn\sigma}\frac{1}{(kr)^{n+1}}P_n^m(\cos\theta)\times\begin{Bmatrix}\cos(m\phi)\\ \sin(m\phi)\end{Bmatrix}, \tag{A1}$$

$$\mathbf{v}_{\text{sc}_l}(\mathbf{r})=\sum_{n=0}^{\infty}\sum_{m=0}^{n}\sum_{\sigma=e,o} A^3_{mn\sigma}\left[\frac{1}{(kr)^{n+2}}\right]\left[-(n+1)P_n^m(\cos\theta)\times\begin{Bmatrix}\cos(m\phi)\\ \sin(m\phi)\end{Bmatrix}\hat{\mathbf{r}}\right.$$
$$\left.+\frac{dP_n^m(\cos\theta)}{d\theta}\times\begin{Bmatrix}\cos(m\phi)\\ \sin(m\phi)\end{Bmatrix}\hat{\theta}+\frac{mP_n^m(\cos\theta)}{\sin\theta}\times\begin{Bmatrix}-\sin(m\phi)\\ \cos(m\phi)\end{Bmatrix}\hat{\phi}\right], \tag{A2}$$

and

$$\mathbf{v}_{\text{sc}_l}(\mathbf{r})=\sum_{n=1}^{\infty}\sum_{m=0}^{n}\sum_{\sigma=e,o}\left[C^3_{mn\sigma}n(n+1)\frac{h_n(kr)}{kr}P_n^m(\cos\theta)\times\begin{Bmatrix}\cos(m\phi)\\ \sin(m\phi)\end{Bmatrix}\right]\hat{\mathbf{r}}$$
$$+\left[B^3_{mn\sigma}h_n(kr)\frac{mP_n^m(\cos\theta)}{\sin\theta}\times\begin{Bmatrix}-\sin(m\phi)\\ \cos(m\phi)\end{Bmatrix}+C^3_{mn\sigma}\frac{1}{kr}\frac{d}{dr}[rh_n(kr)]\frac{dP_n^m(\cos\theta)}{d\theta}\times\begin{Bmatrix}\cos(m\phi)\\ \sin(m\phi)\end{Bmatrix}\right]\hat{\theta}$$
$$+\left[-B^3_{mn\sigma}h_n(kr)\frac{dP_n^m(\cos\theta)}{d\theta}\times\begin{Bmatrix}\cos(m\phi)\\ \sin(m\phi)\end{Bmatrix}+C^3_{mn\sigma}\frac{1}{kr}\frac{d}{dr}[rh_n(kr)]\frac{mP_n^m(\cos\theta)}{\sin\theta}\times\begin{Bmatrix}-\sin(m\phi)\\ \cos(m\phi)\end{Bmatrix}\right]\hat{\phi}. \tag{A3}$$

When the summation index σ is even (e), the upper function in curly brackets is used and when σ is odd (o), the lower function is used. The associated Legendre functions are denoted by $P_n^m(\cos\theta)$. In the forward direction only the $m=1$ terms in the scattered velocity expansions survive, while both the $m=0$ and 1 terms survive in the expansion for the scattered pressure.

In the far zone the functional kr dependences can be simplified by utilizing the following asymptotic tendencies of the spherical Hankel functions:

$$h_n(kr)\underset{|k|r\gg 1}{\sim}\frac{e^{ikr}}{kr}i^{-(n+1)}+O\left[\frac{1}{(kr)^2}\right],$$
$$\frac{1}{kr}\frac{d}{dr}[rh_n(kr)]\underset{|k|r\gg 1}{\sim}\frac{e^{ikr}}{kr}i^{-n}+O\left[\frac{1}{(kr)^2}\right].$$

From the far-zone approximation of $\mathbf{v}_{\text{sc}}$ the kr dependence [shown in (28)] can now be factored out from (A1)–(A3), yielding two vector sums involving only the angular functions:

$$\mathbf{g}_1(\hat{\mathbf{r}})=\sum_{n=1}^{\infty}\sum_{m=0}^{n}\sum_{\sigma=e,o}\left[B^3_{\sigma mn}i^{-(n+1)}\frac{mP_n^m(\cos\theta)}{\sin\theta}\times\begin{Bmatrix}-\sin(m\phi)\\ \cos(m\phi)\end{Bmatrix}+C^3_{\sigma mn}i^{-n}\frac{dP_n^m(\cos\theta)}{d\theta}\times\begin{Bmatrix}\cos(m\phi)\\ \sin(m\phi)\end{Bmatrix}\right]\hat{\theta}$$
$$+\left[-B^3_{\sigma mn}i^{-(n+1)}\frac{dP_n^m(\cos\theta)}{d\theta}\times\begin{Bmatrix}\cos(m\phi)\\ \sin(m\phi)\end{Bmatrix}+C^3_{\sigma mn}i^{-n}\frac{mP_n^m(\cos\theta)}{\sin\theta}\times\begin{Bmatrix}-\sin(m\phi)\\ \cos(m\phi)\end{Bmatrix}\right]\hat{\phi}, \tag{A4}$$

$$\mathbf{g}_2(\hat{\mathbf{r}})=\sum_{n=1}^{\infty}\sum_{m=0}^{n}\sum_{\sigma=e,o}\left[B^3_{\sigma mn}ki^{-n}\frac{mP_n^m(\cos\theta)}{\sin\theta}\times\begin{Bmatrix}-\sin(m\phi)\\ \cos(m\phi)\end{Bmatrix}+C^3_{\sigma mn}ki^{-n+1}\frac{dP_n^m(\cos\theta)}{d\theta}\times\begin{Bmatrix}\cos(m\phi)\\ \sin(m\phi)\end{Bmatrix}\right]\hat{\theta}$$
$$+\left[-B^3_{\sigma mn}ki^{-n}\frac{dP_n^m(\cos\theta)}{d\theta}\times\begin{Bmatrix}\cos(m\phi)\\ \sin(m\phi)\end{Bmatrix}+C^3_{\sigma mn}ki^{-n+1}\frac{mP_n^m(\cos\theta)}{\sin\theta}\times\begin{Bmatrix}-\sin(m\phi)\\ \cos(m\phi)\end{Bmatrix}\right]\hat{\phi}\ . \tag{A5}$$

Also, from the far-zone approximation for pressure we are able to define the constant $D'=kA^3_{e00}$.

With the detector placed in the forward scattering direction, the assumption that $\Omega_d \ll 1$ entails $\hat{\mathbf{r}}=\hat{\mathbf{z}}$ and $\theta=0$. Since $[dP_n^1(\cos\theta)/d\theta]_{\theta=0}=[P_n^1(\cos\theta)/\sin\theta]_{\theta=0}=n(n+1)/2$, we get

$$\mathbf{g}_1(\hat{\mathbf{z}})=\sum_{n=1}^{\infty}\frac{n(n+1)}{2}i^{-n}\{(-iB^3_{o1n}+C^3_{e1n})\hat{\mathbf{x}}+(iB^3_{e1n}+C^3_{o1n})\hat{\mathbf{y}}\}=\sum_{n=1}^{\infty}\mathbf{g}_{1_n}\ , \tag{A6}$$

$$\mathbf{g}_2(\hat{\mathbf{z}})=k\sum_{n=1}^{\infty}\frac{n(n+1)}{2}i^{-n}\{(B^3_{o1n}+iC^3_{e1n})\hat{\mathbf{x}}+(-B^3_{e1n}+iC^3_{o1n})\hat{\mathbf{y}}\}\ . \tag{A7}$$

Hence $\mathbf{g}_2(\hat{\mathbf{z}})=ik\mathbf{g}_1(\hat{\mathbf{z}})$. In practice the summation index n extends only over some finite range $1\le n\le N$, where N is large enough so that the series in (A6) converges to within a desired tolerance limit.

The incident velocity phasor can be expanded in terms of spherical harmonic functions [18] that are regular at the origin as

$$\mathbf{v}_i(\mathbf{r})=\sum_{n=1}^{\infty}\sum_{m=0}^{n}\sum_{\sigma=e,o}\left[C^1_{mn\sigma}n(n+1)\frac{j_n(kr)}{kr}P_n^m(\cos\theta)\times\begin{Bmatrix}\cos(m\phi)\\ \sin(m\phi)\end{Bmatrix}\right]\hat{\mathbf{r}}$$
$$+\left[B^1_{mn\sigma}j_n(kr)\frac{mP_n^m(\cos\theta)}{\sin\theta}\times\begin{Bmatrix}-\sin(m\phi)\\ \cos(m\phi)\end{Bmatrix}+C^1_{mn\sigma}\frac{1}{kr}\frac{d}{dr}[rj_n(kr)]\frac{dP_n^m(\cos\theta)}{d\theta}\times\begin{Bmatrix}\cos(m\phi)\\ \sin(m\phi)\end{Bmatrix}\right]\hat{\theta}$$
$$+\left[-B^1_{mn\sigma}j_n(kr)\frac{dP_n^m(\cos\theta)}{d\theta}\times\begin{Bmatrix}\cos(m\phi)\\ \sin(m\phi)\end{Bmatrix}+C^1_{mn\sigma}\frac{1}{kr}\frac{d}{dr}[rj_n(kr)]\frac{mP_n^m(\cos\theta)}{\sin\theta}\times\begin{Bmatrix}-\sin(m\phi)\\ \cos(m\phi)\end{Bmatrix}\right]\hat{\phi}\ , \tag{A8}$$

in which the only nonzero incident expansion coefficients are $B^1_{1no}=i^n[(2n+1)/n(n+1)]V$ and $C^1_{1ne}=-iB^1_{1no}$ when $\mathbf{v}_i(\hat{\mathbf{r}})=V\hat{\mathbf{x}}e^{ikz}$.

[1] M. J. Marcinkowski, Acta Phys. Pol. A **81**, 543 (1992).

[2] *Field Representations and Introduction to Scattering,* edited by V. V. Varadan, A. Lakhtakia, and V. K. Varadan (North-Holland, Amsterdam, 1991).

[3] B. U. Felderhof, Physica A **84**, 557 (1976).

[4] B. U. Felderhof, Physica A **84**, 569 (1976).

[5] R. Schmitz and B. U. Felderhof, Physica A **113**, 90 (1982).

[6] B. U. Felderhof, Physica A **136**, 77 (1986).

[7] J. Happel and H. Brenner, *Low Reynolds Number Hydrodynamics* (Noordhoff, Leyden, 1973).

[8] H. Lamb, *Hydrodynamics* (Dover, New York, 1945).

[9] B. Padmavathi, T. Amarnath, and S. D. Nigam, Fluids Dyn. Res. **11**, 229 (1993).

[10] A. T. de Hoop, Appl. Sci. Res. B **7**, 463 (1959).

[11] D. S. Jones, *Acoustic and Electromagnetic Waves* (Oxford University Press, Oxford, 1986).

[12] H. C. van de Hulst, *Light Scattering by Small Particles* (Dover, New York, 1981).

[13] C. F. Bohren and D. P. Gilra, J. Colloid Interface Sci. **72**, 215 (1979).

[14] A. Lakhtakia, Optik **99**, 35 (1995).

[15] W. O. Criminale and F. J. P. Smith, Fluid Dyn. Res. **13**, 167 (1994).

[16] M. Born and E. Wolf, *Principles of Optics,* 6th ed. (Pergamon, Oxford, 1987).

[17] *Handbook of Mathematical Functions,* edited by M. Abramowitz and I. A. Stegun (Dover, New York, 1972).

[18] P. M. Morse and M. Feshbach, *Methods of Theoretical Physics* (McGraw-Hill, New York, 1953), Vol. II.